Supporting Information

Metal-Organic Framework Nanoparticle-Assisted Cryopreservation of Red Blood Cells

Wei Zhu,[a,‡] Jimin Guo,[a,‡] Jacob Ongudi Agola,[a] Jonas G. Croissant,[a] Zihao Wang,[a] Jin Shang,[b] Eric Coker,[c] Benyamin Motevalli,[d] Andreas Zimpel,[e] Stefan Wuttke,[e,f] and C. Jeffrey Brinker [a,*]

[a] Center for Micro-Engineered Materials, Department of Chemical and Biological Engineering, the University of New Mexico, Albuquerque, New Mexico 87131 (USA)

[b] School of Energy and Environment, City University of Hong Kong, Tat Chee Avenue, Kowloon, Hong Kong SAR (P. R. China)

[c] Sandia National Laboratories, Applied Optical/Plasma Sciences, PO Box 5800, MS 1411, Albuquerque NM 87185-1411 (USA)

[d] Department of Mechanical and Aerospace Engineering, Monash University, Clayton, Victoria 3800, (Australia)

[e] Department of Chemistry and Center for NanoScience (CeNS), University of Munich (LMU), 81377 Munich (Germany)

[f] School of Chemistry, Joseph Banks Laboratories, University of Lincoln, Lincoln LN6 7TS (UK)

TABLE OF CONTENT

Section S1. General information

Reagents. All chemicals and reagents were used as received. Zirconium(IV) chloride, terephthalic acid, 2-aminoterephthalic acid, 2,5-dihydroxyterephthalic acid, dimethyl-formamide (DMF), trimesic acid, biphenyl-4,4'-dicarboxylic acid, formaldehyde solution (36.5-38% in H_2O) were purchased from Sigma-Aldrich. Phosphate-buffered saline (1x PBS) was purchased from Thermo Fisher Scientific while milli-Q water with a resistivity of 18.2 MΩ cm was obtained from a Millipore RiOs/Origin water purification system.

Characterization. The morphology of the MOF nanoparticles (NPs) was characterized using a Hitachi SU-8010 field-emission scanning electron microscope (SEM) operating at an accelerating voltage of 20 kV and a Hitachi model H-7650 transmission electron microscope (TEM) operating at 200 kV. Wide-angle powder X-ray diffraction (PXRD) patterns were measured using the D/max- RB (Japan, Rigaku) diffractometer with monochromatized Cu Kα radiation (λ=0.15418 nm), operating at 40 KV and 120 mA. Argon adsorption−desorption isotherms were obtained using a Quantachrome ASiQ2 instrument operating at 87 K. For DFT calculations, Quantachrome's Quenched Solid DFT (QSDFT) model for the adsorption branch of Ar at 87 K on carbons with cylindrical/spherical pores was used, while fluorescent images were acquired using a Zeiss LSM 510 META (Carl Zeiss MicroImaging, Inc.; Thornwood, NY, USA) microscope operated in channel mode using the Zeiss LSM 510 software.

Section S2. MOF NP synthesis

UiO-66/ UiO-67/ UiO-66-OH NP synthesis. UiO-66 NPs were synthesized following the previously reported methods without any modification.[1] Briefly, 25.78 mg $ZrCl_4$ (0.11 mmol final) and 13.29 mg 1,4-benzenedicarboxylic acid (0.08 mmol final) were dissolved in 10 mL of DMF solvent. Then 1.441 g acetic acid (0.024 M final) was added to the above solution. The mixture was then placed in an oven (120 °C) for 24 h. After the reaction mixture was cooled to room temperature, the resultant NPs were washed with DMF and methanol via centrifugation-redispersion cycles. The synthesized UiO-66 NPs were then stored in ethanol before use. For the synthesis of UiO-66-OH, and UiO-67, a similar protocol was used except that the organic ligand 1,4-benzenedicarboxylic acid

was replaced with 2,5-dihydroxyterephthalic acid and biphenyl-4,4'-dicarboxylic acid respectively.

UiO-66-NH_2 NP (230 nm) synthesis. Briefly, 51.56 mg $ZrCl_4$ (0.22 mmol final) and 14.48 mg 2-amino terephthalic acid (0.08 mmol final) were dissolved in 10 mL of DMF solvent. Then 1.372 mL acetic acid (0.024 M final) was added to the above solution. The mixture was then placed in an oven (110 °C) for 24 h. After the reaction mixture was cooled to room temperature, the resultant NPs were washed with DMF and methanol via centrifugation-redispersion cycles.

UiO-66-NH_2 NP (440 nm) synthesis. Briefly, 25.78 mg $ZrCl_4$ (0.11 mmol final) and 14.48 mg 2-amino terephthalic acid (0.08 mmol final) were dissolved in 10 mL of DMF solvent. Then 1.372 mL acetic acid (0.024 M final) was added to the above solution. The mixture was then placed in an oven (120 °C) for 24 h. After the reaction mixture was cooled to room temperature, the resultant NPs were washed with DMF and methanol via centrifugation-redispersion cycles.

UiO-66-NH_2 NP (800nm) synthesis. Briefly, 5mg UiO66-NH_2 nanoparticle (440 nm), 25.78 mg $ZrCl_4$ (0.11 mmol final) and 14.48 mg 2-amino terephthalic acid (0.08 mmol final) were dissolved in 10 mL of DMF solvent. Then 1.372 mL acetic acid (0.024 M final) was added to the above solution. The mixture was then placed in oil bath (110 °C) under stirring for 24 h. After the reaction mixture was cooled to room temperature, the resultant NPs were washed with DMF and methanol via centrifugation-redispersion cycles.

MOF-808 NP synthesis. MOF-808 NPs were synthesized following the previously reported method with no modification.[2] Briefly, 0.11g H_3BTC (0.50 mmol final) and 0.16 g $ZrOCl_2 \cdot 8H_2O$ (0.50 mmol final) were dissolved in 40 mL of mixed DMF/formic acid solution (20 mL/20 mL). The mixture was then placed in an oven (100 °C) for 48 h. After the solution was cooled to room temperature, the resultant NPs were subsequently washed with DMF and methanol via centrifugation-redispersion cycles. The synthesized MOF-808 NPs were then stored in ethanol before the successive use.

Section S3. UiO-66-NH_2 NPs with different surface charges

For the surface modification of UiO66-NH_2 NPs, 3mg UiO66-NH_2 nanoparticle and different amount of phosphocholine chloride calcium salt tetrahydrate (10 mg or 15 mg) were dissolved in 3mL of DMF solvent. The mixture was then maintained under stirring for 24 h. The resultant NPs were washed with DMF, methanol, 1X PBS (pH7.4) and water via centrifugation-redispersion cycles.

Section S4. Hemolysis Assay

The purified RBCs were incubated with different concentrations of MOF nanoparticles at room temperature for 2 h in a continuous rotating state. Double distilled (D.I.) water and 1x PBS containing purified RBCs were used as the positive and negative controls, respectively. Finally, the mixtures were centrifuged at 300g for 3 min, and then 100 µl of the sample supernatant was transferred to a 96-well plate. The absorbance of hemoglobin in the supernatant was then measured on a BioTek microplate reader (Winooski, VT) at 540 nm. The hemolysis percentage of each sample was calculated using the standard equation; Percent hemolysis (%) = 100 × (Sample Abs_{540nm}-Negative control Abs_{540nm}) / (Positive control Abs_{540nm}-Negative control Abs_{540nm}).

Section S5. “Splat” Assay study

The ice recrystallization inhibition properties of various MOF NPs were examined using the “splat” assay experiment. The “splat” assay involves dropping a ~10 µL droplet from a height of approximately 2 m onto a coverslip, previously cooled to −80 °C. The coverslip is then annealed at −6 °C or at varied temperatures from -10 °C to -2 °C for different times under an optical microscope. The largest dimension of the 10 largest ice crystals from each image is then measured using appropriate software such as Image J.

Section S6. Freezing and Thawing of Erythrocytes

A freshly prepared RBC suspension was frozen by immersion in liquid N_2 (−196 °C) for a period of 10 min and then kept in liquid N_2 for two days. Thawing of the RBC samples

was then carried out at 4 °C for a couple of hours until all the ice had melted. The RBC recovery was then calculated using the same formula used for the hemolysis in section S3.

Section S7. Calculation of the Surface Matching at the Interface of Ice Plane and MOF (111) Surface

The ice plane and MOF (111) surface matching at the interface was calculated using MATLAB software. The lattice structures of oxygen atoms belonging to water molecules on the top surface of the ice planes and the carboxylic groups of the organic linkers on the top surface of MOF (111) surfaces, were used for the surface matching calculation. The ice plane was fixed, and the MOF (111) surface was then rotated around one oxygen atom on the ice plane. The rotation step was set at 2°. At each step, the Euclidean distances of O---O between all the oxygen atoms on the ice planes and MOF (111) surfaces was calculated and counted. The cut-off distance of O---O was set as 3.5 Å (2.5 Å+O-H bond; where 2.5 Å corresponds to the maximum distance of a hydrogen bond). The maximum matching number of O···O between the ice plane and the MOF (111) surface was calculated using:

$$N_{total}=0.25\times N_{vertex}+0.5\times N_{Surface}+N_{Interior}$$

N_{total} is the maximum matching number of O···O between the ice plane and MOF (111) surface, N_{vertex} is the matching number coming from the oxygen atoms at the vertex of the parallelogram (Scheme S1), $N_{surface}$ is matching number for the oxygen atoms at the side of the parallelogram, and $N_{Interior}$ is matching number for the oxygen atoms inside the parallelogram. Note that due to hydrogen bonding being directional, the matching number in this case is only a qualitative description of the two-plane fitting and not representative of the exact number of hydrogen bonds at the ice and MOF interface.

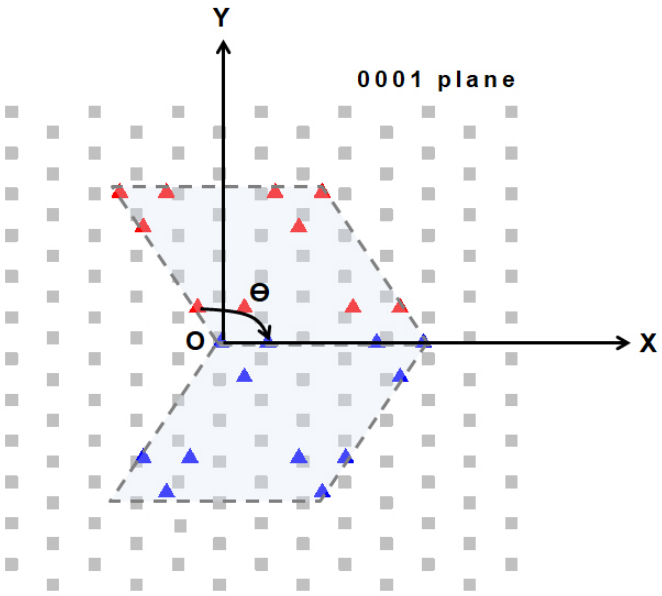

Scheme S1 | Schematic illustration of the fitting process at the interface of ice plane and the MOF (111) surface.

Section S8. Supplementary Figures

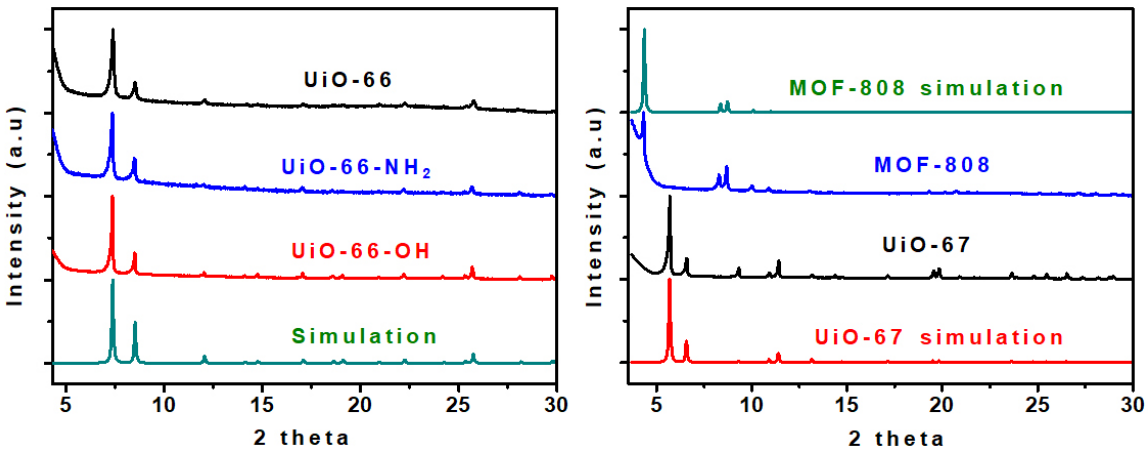

Figure S1 | Wide angle PXRD patterns of the as-synthesized MOF NPs relative to the simulated ones.

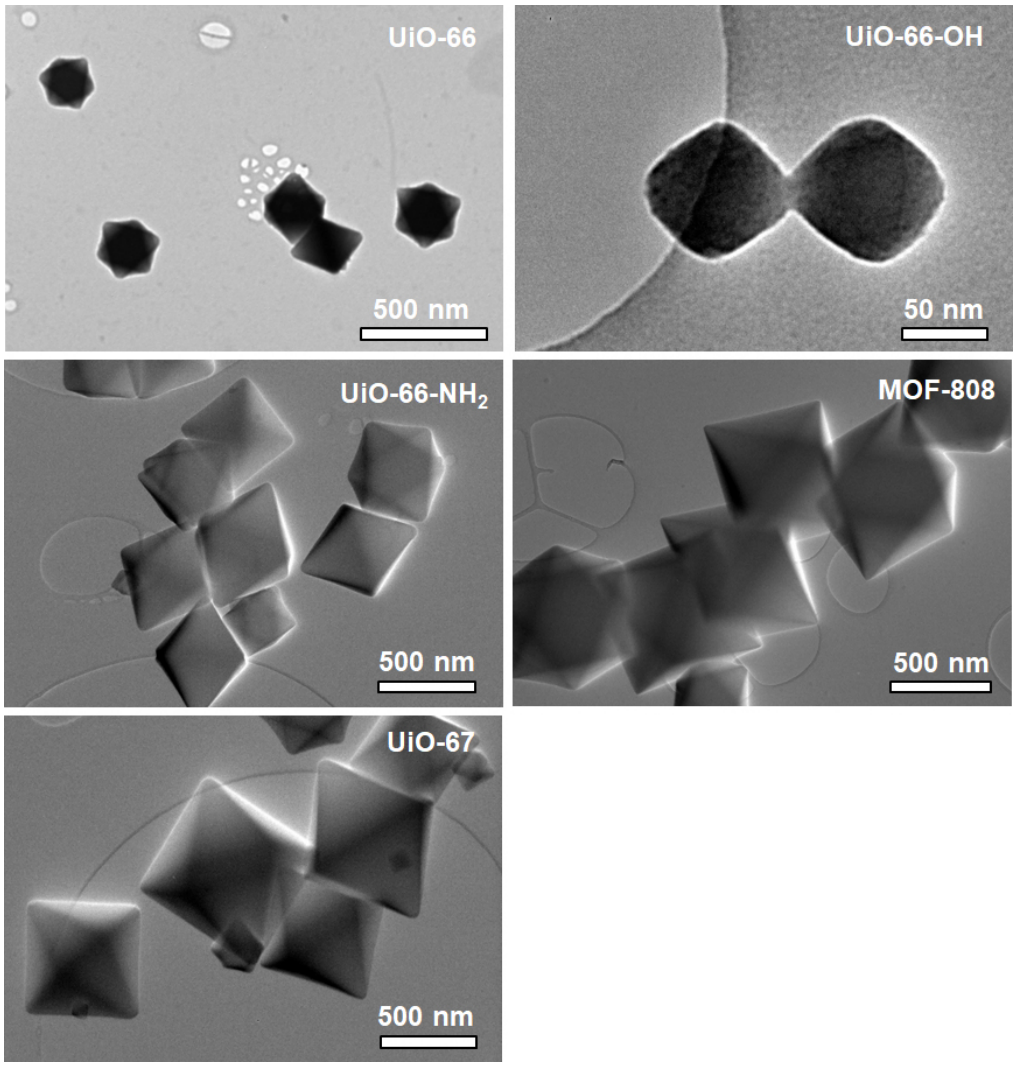

Figure S2 | TEM images of the synthesized Zr-MOF NPs.

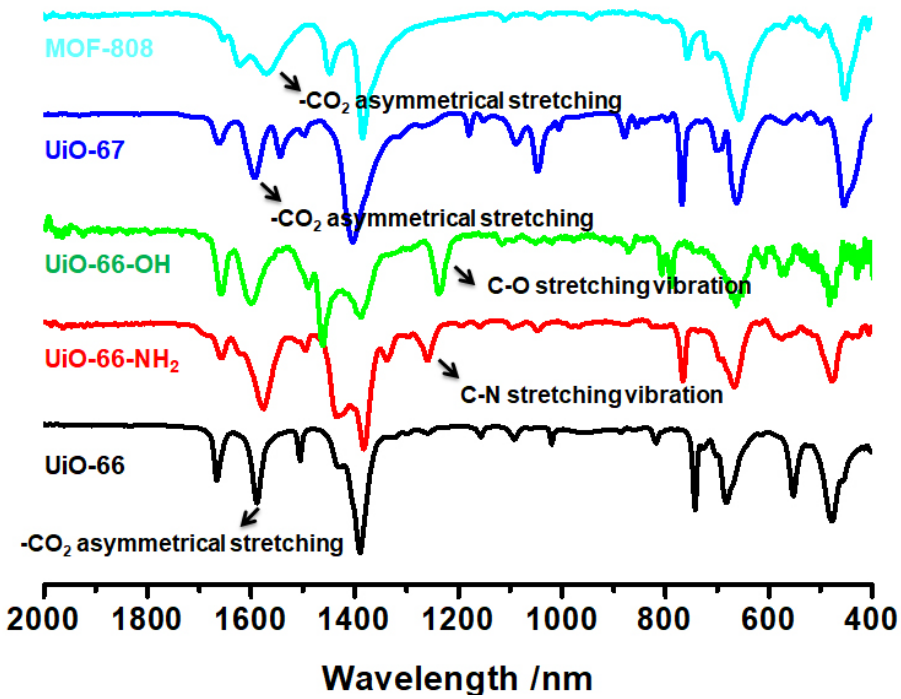

Figure S3 | FTIR spectra of the MOF NPs of UiO-66, UiO-66-NH_2, UiO-66-OH, UiO-67, and MOF-808 showing characteristic functional ligand vibrations of the respective MOFs.

	UiO-66	UiO-66-NH_2	UiO-66-OH	UiO-67	MOF-808
Zeta potential /mV	-9.4	-29.1	-15.4	-16.3	-14.4

Figure S4 | Measured zeta potential values of the Zr-MOF NPs.

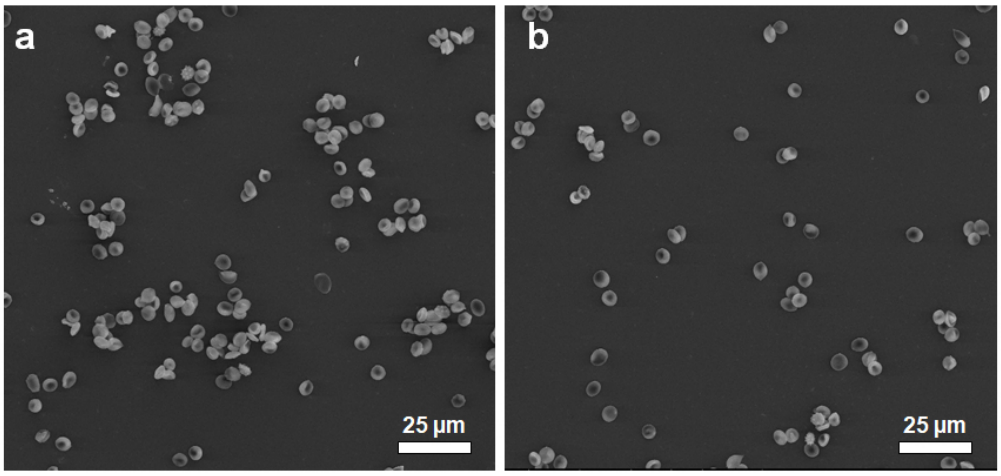

Figure S5 | SEM images of human RBCs before (a) and after (b) cryopreservation.

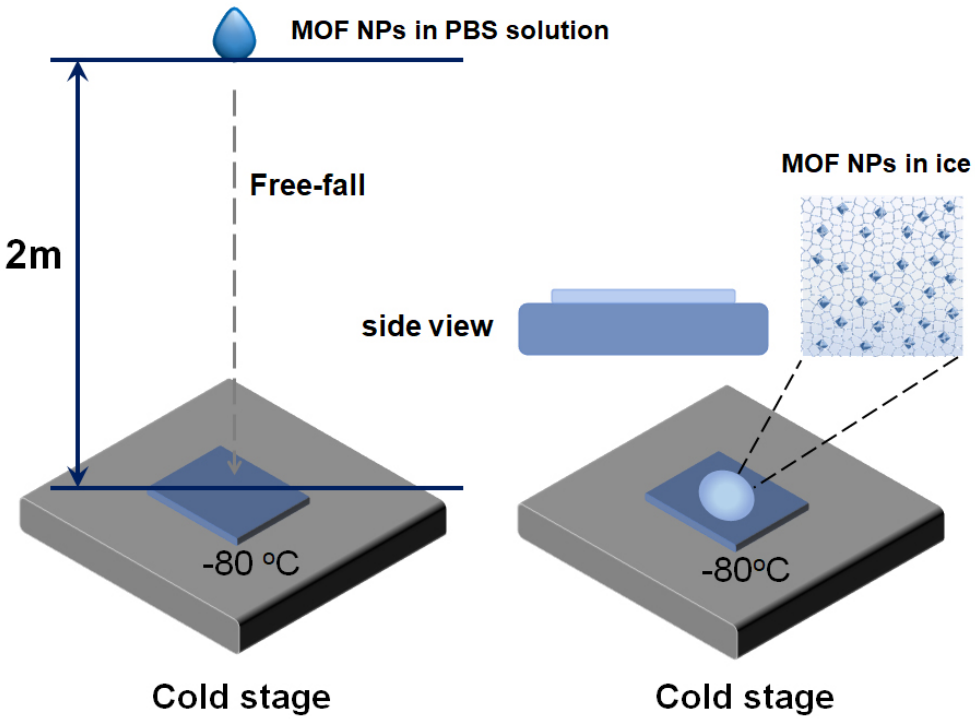

Figure S6 | Schematic illustration of the 'splat assay' process.

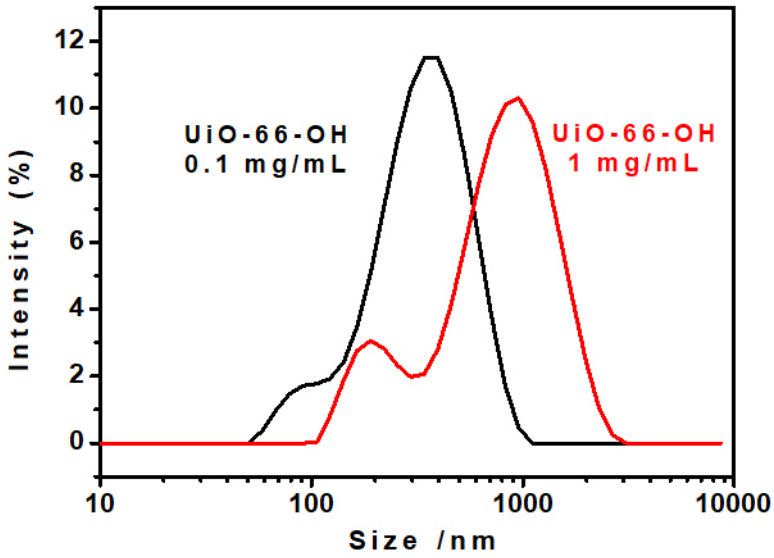

Figure S7 | Dynamic light scattering **(**DLS) size distribution of UiO-66-OH MOF NPs suspended in 1x PBS solution at different concentrations.

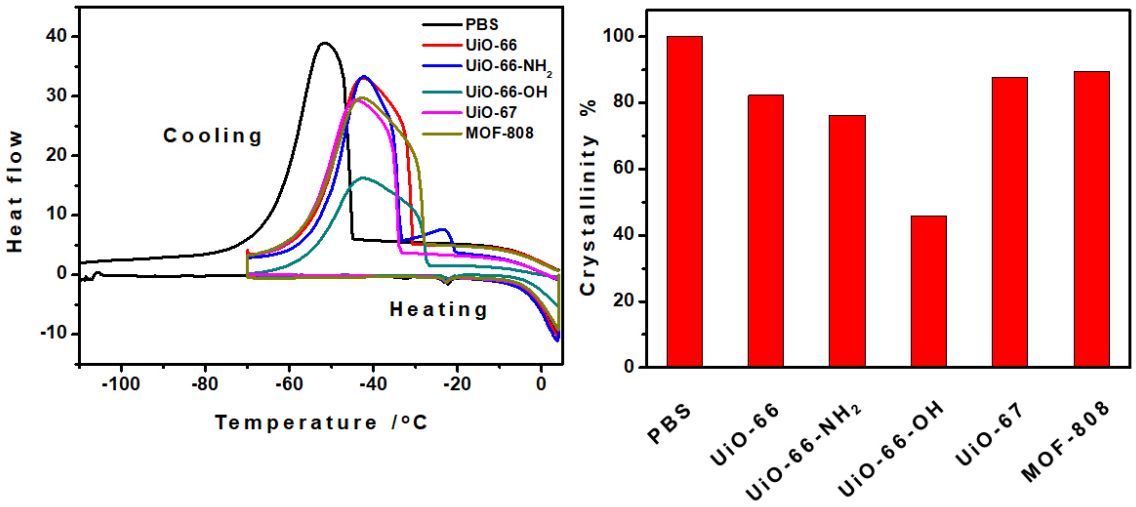

Figure S8 | Differential scanning calorimetry **(**DSC) analysis of the freeze−thawing of MOF NPs (1 mg mL^{-1}) in PBS solutions. Samples were cooled and heated at 20 °C min^{-1} and 2 °C min^{-1}, respectively (left). The crystallinity of ice crystals in MOF NP-containing PBS solutions (right).

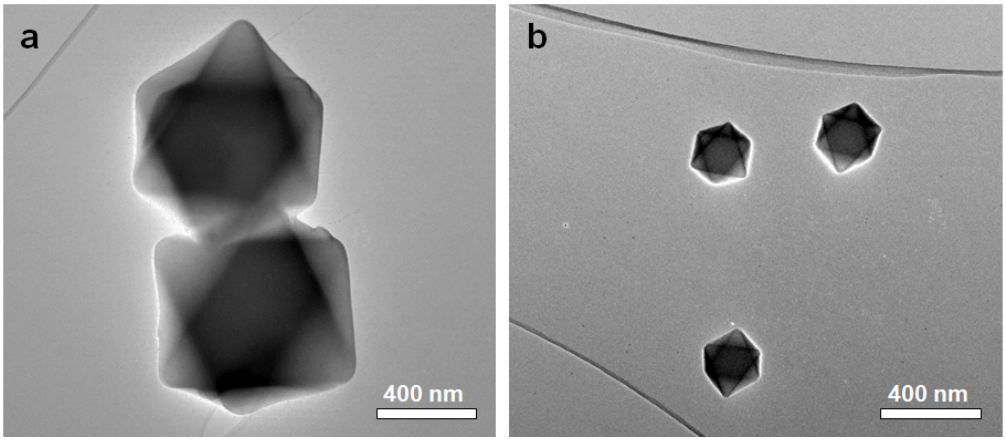

Figure S9 | SEM images of UiO-66-NH_2 MOF NPs with different sizes of ~ 800 nm (a) and 230 nm (b).

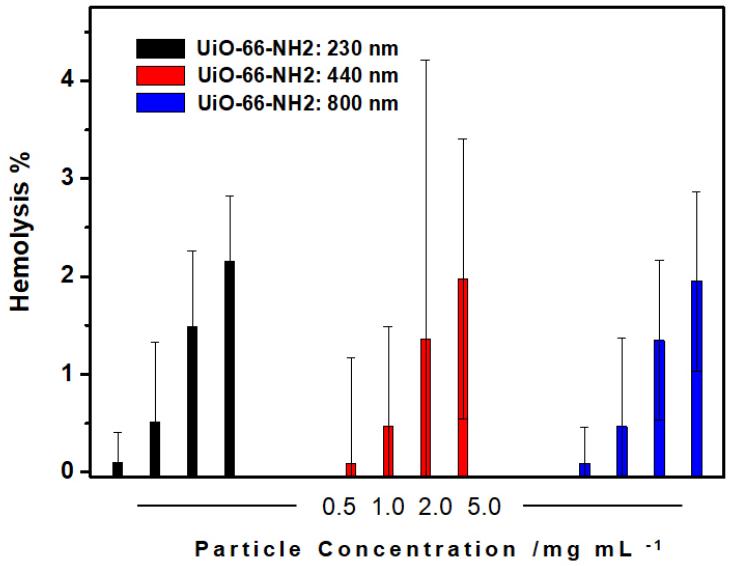

Figure S10 | Percent hemolysis of human RBCs upon incubation with UiO-66 NH_2 MOF NPs with different sizes of 230 nm, 440nm, and 800 nm.

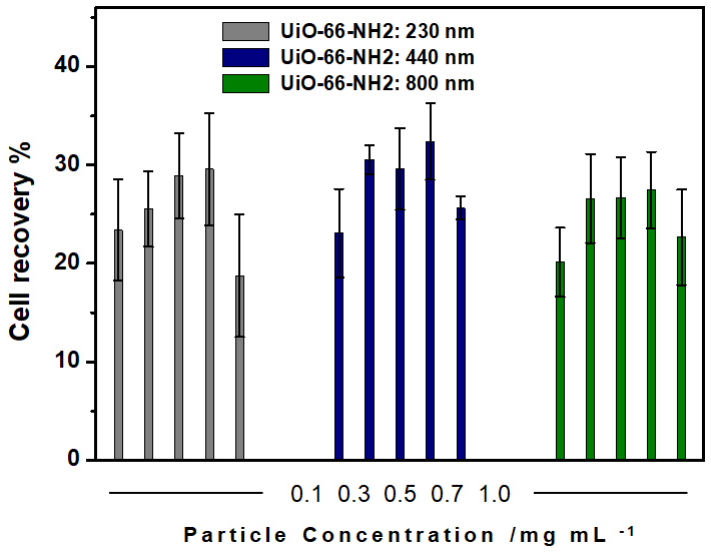

Figure S11 | The recovery of human RBCs cryopreserved in MOF NP PBS dispersions with different sizes and under a stringent test condition of slow thawing at 4 °C.

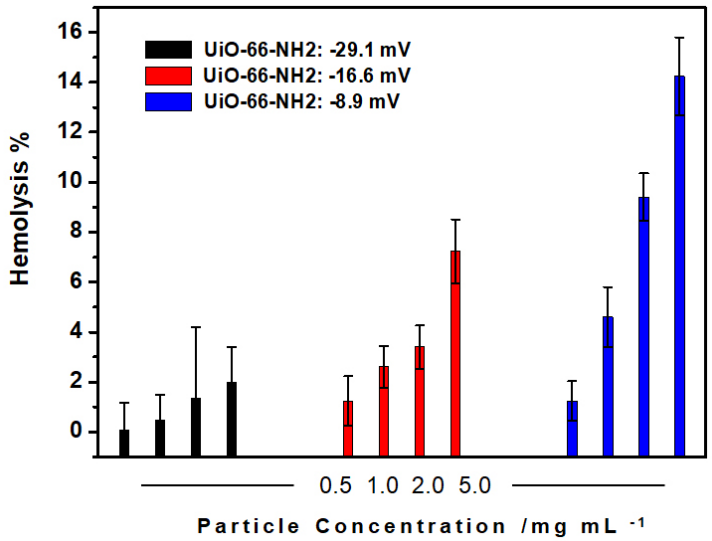

Figure S12 | Percent hemolysis of human RBCs upon incubation with UiO-66 NH_2 MOF NPs with different zeta potentials of -29.1 mV, -16.6 mV, and -8.9 mV.

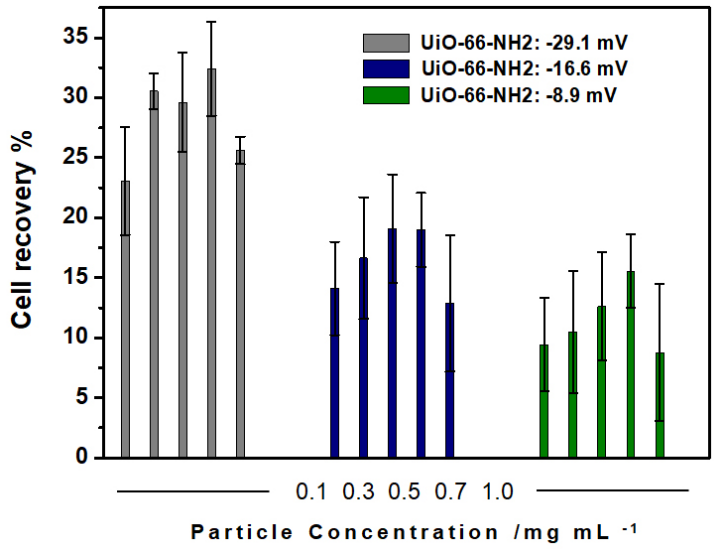

Figure S13 | The recovery of human RBCs cryopreserved in MOF NP PBS dispersions with different zeta potentials and under a stringent test condition of slow thawing at 4 °C.

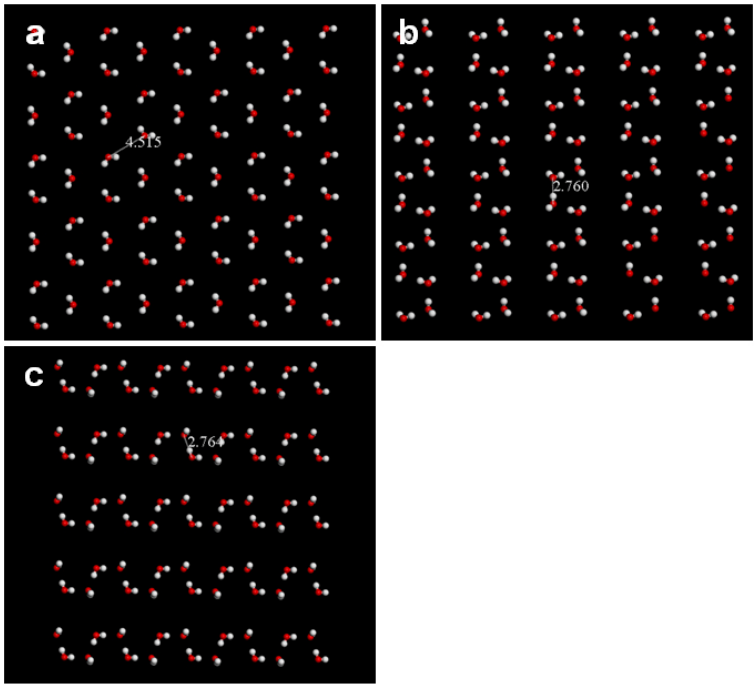

Figure S14 | Schematic illustration of the water molecules packing on the top basal surface of (a), primary prism (b), secondary prism, and (c) plane.

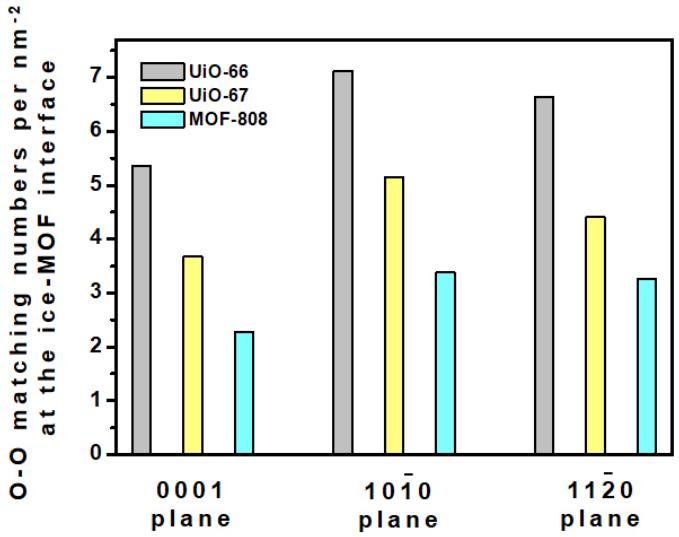

Figure S15 | The maximum matching numbers per nm^{-2} of O-O from the ice planes and MOF (111) planes at the interface.

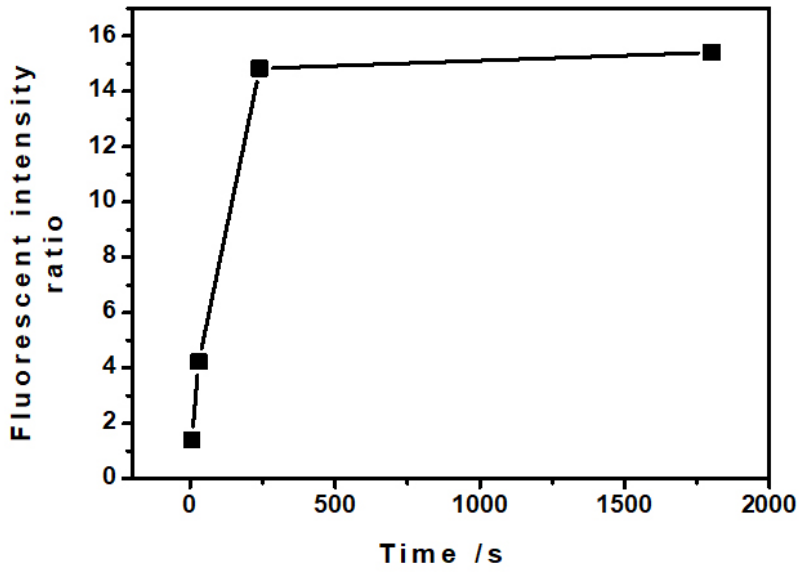

Figure S16 | Time-dependent fluorescent intensity ratio between the ice edge area and the middle ice crystals.

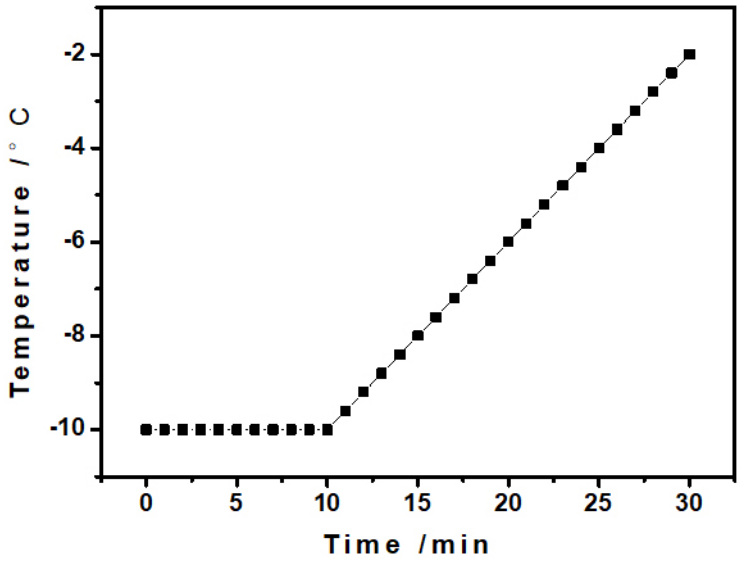

Figure S17 | Temperature variation of the cold stage used for the ice recrystallization study.

Section S9. Supplementary References

1. Lu, G.; Cui, C.; Zhang, W.; Liu, Y. & Huo, F. Synthesis and Self-Assembly of Monodispersed Metal-Organic Framework Microcrystals. *Chem. Asian J.* **8**, 69-72 (2013). DOI: 10.1002/asia.201200754

2. Furukawa, H.; Gándara, F.; Zhang, Y.; Jiang, J.; Queen, W. L.; Hudson, M. & Yaghi, O. M. Water Adsorption in Porous Metal−Organic Frameworks and Related Materials. *J. Am. Chem. Soc.* **136**, 4369−4381 (2014). **DOI:** 10.1021/ja500330a